Protein Science (1994), *3*:1504-1514. Cambridge University Press. Printed in the USA.

Anatomy of an engineered NAD-binding site

P.R.E. MITTL,[1] A. BERRY,[2] N.S. SCRUTTON,[2] R.N. PERHAM,[2] AND G.E. SCHULZ[1]

[1] Institut für Organische Chemie und Biochemie, Albert-Ludwigs-Universität, Albertstrasse 21, 79104 Freiburg im Breisgau, Germany

[2] Cambridge Centre for Molecular Recognition, Department of Biochemistry, University of Cambridge, Tennis Court Road, Cambridge CB2 1QW, United Kingdom

(RECEIVED March 9, 1994; ACCEPTED June 13, 1994)

Abstract

The coenzyme specificity of *Escherichia coli* glutathione reductase was switched from NADP to NAD by modifying the environment of the 2′-phosphate binding site through a set of point mutations: A179G, A183G, V197E, R198M, K199F, H200D, and R204P (Scrutton NS, Berry A, Perham RN, 1990, *Nature 343*:38-43). In order to analyze the structural changes involved, we have determined 4 high-resolution crystal structures, i.e., the structures of the wild-type enzyme (1.86 Å resolution, *R*-factor of 16.8%), of the wild-type enzyme ligated with NADP (2.0 Å, 20.8%), of the NAD-dependent mutant (1.74 Å, 16.8%), and of the NAD-dependent mutant ligated with NAD (2.2 Å, 16.9%). A comparison of these structures reveals subtle differences that explain details of the specificity change. In particular, a peptide rotation occurs close to the adenosine ribose, with a concomitant change of the ribose pucker. The mutations cause a contraction of the local chain fold. Furthermore, the engineered NAD-binding site assumes a less rigid structure than the NADP site of the wild-type enzyme. A superposition of the ligated structures shows a displacement of NAD versus NADP such that the electron pathway from the nicotinamide ring to FAD is elongated, which may explain the lower catalytic efficiency of the mutant. Because the nicotinamide is as much as 15 Å from the sites of the mutations, this observation reminds us that mutations may have important long-range consequences that are difficult to anticipate.

Keywords: coenzyme specificity change; glutathione reductase; NAD-binding site; NADP-binding site; protein engineering

The coenzyme NADP differs from NAD by virtue of its additional 2′-phosphate at the adenosine ribose. These ubiquitous dinucleotides undergo redox reactions with distinct metabolic functions. NAD participates mostly in catabolic reactions, for instance, NADH is a fuel for the regeneration of ATP in oxidative phosphorylation. In contrast, NADPH provides redox equivalents for anabolic reactions, as for example in lipid biosynthesis. In keeping with this, glutathione reductase from *Escherichia coli* (EC 1.6.4.2) is an FAD-dependent homodimeric enzyme with an M_r of 49,560 per subunit that catalyzes the reduction of oxidized glutathione at the expense of NADPH according to the equation: NADPH + GSSG + H^+ ⇌ $NADP^+$ + 2GSH.

Scrutton et al. (1990) created an NAD-dependent mutant of GR_{eco} by the introduction of 7 point mutations (A179G, A183G, V197E, R198M, K199F, H200D, and R204P) in the $\beta\alpha\beta\alpha\beta$-motif of the coenzyme-binding domain. These are the residues at the equivalent positions in the homologous NAD-dependent dihydrolipoamide dehydrogenase from *E. coli* (28% sequence identity; Stephens et al., 1983). We have now determined the 3-dimensional structures of the wild-type GR_{eco} (hereafter designated as "Wild-type") and of the NAD-dependent mutant (designated "Mutant"), with and without the bound dinucleotides. The 4 structures have been established at high resolution by X-ray crystallography, which is a prerequisite for analyzing any small changes in structure and mobility (see Kinemage 1).

The analysis points to certain essential features of NAD(P)-binding at the $\beta\alpha\beta\alpha\beta$-motif of a "Rossmann fold," which continues to be a subject of widespread discussion (Wierenga et al., 1986; Hanukoglu & Gutfinger, 1989; Baker et al., 1992; Mattevi et al., 1992; Schulz, 1992; Bocanegra et al., 1993; Mittl et al., 1993; Rescigno & Perham, 1994). NAD(P)-binding sites are sufficiently well documented that in many cases they can be detected from the amino acid sequence. Accordingly, there is reason to hope that a change of coenzyme specificity might be achieved in an enzyme even without an X-ray structure determination. This could become of commercial importance if biosynthetic enzymes using expensive NADPH could be replaced

Reprint requests to: G.E. Schulz, Institut für Organische Chemie und Biochemie, Albertstrasse 21, 79104 Freiburg im Breisgau, Germany; e-mail: schulz@bio2.chemie.uni-freiburg.de.

Abbreviations: GR_{eco}, glutathione reductase from *Escherichia coli*; Wild-type, native GR_{eco}; Mutant, NAD-dependent GR_{eco} with 7 point mutations; σ, standard deviation; NAD, NAD^+ or NADH; NADP, $NADP^+$ or NADPH; NAD(P), all 4 forms; PEG, polyethylene glycol.

by appropriately engineered enzymes using the cheaper NADH. These expectations are somewhat muted, however, by the data presented, which point to some general problems in protein engineering that may limit the success rate.

Results and discussion

The 4 underlying structures

In order to identify the structural changes caused by the mutations and to analyze their consequences for coenzyme binding to GR_{eco}, we have determined 4 structures: the Wild-type enzyme without and with bound NADP and the Mutant without and with bound NAD (Kinemage 1). The characteristics of the resulting models are listed in Table 1. Resolutions between 1.74 Å and 2.2 Å were obtained, and the final crystallographic *R*-factors ranged between 16.8% and 20.8% at good geometries, rendering these models capable of revealing fine detail.

The quality of the structure models is demonstrated by Ramachandran plots for the 2 structures with lower resolutions (Fig. 1). These scatter plots show no unusual (ϕ, ψ) angles except for residues 36 and 199, which, however, are in the same unusual region in *human* glutathione reductase (Karplus & Schulz, 1987). The errors of the atomic coordinates can be derived from *R*-factor plots (Fig. 2). The errors are about 0.2 Å for the unligated structures. Because of lower resolution and completeness (see below), the errors of the enzyme:substrate complexes are about 0.3 Å. The error level is confirmed by main-chain comparisons between the crystallographically independent subunits I and II. In all 4 structures, the observed RMS deviations are about 0.3 Å. This constitutes an upper error limit; the real errors of the well-defined regions are indicated by the RMS deviations of FAD, which are as low as 0.1 Å and 0.15 Å for unligated and ligated enzymes, respectively. The bound coenzymes, NAD and NADP, are well-defined in their ($2F_{obs} - F_{calc}$) maps. It should be noted that the X-ray analysis cannot distinguish between $NAD(P)^+$ and NAD(P)H. Therefore, the analyzed complexes could contain $NAD(P)^+$ or NAD(P)H ligated to the reduced enzyme (open redoxactive disulfide is visible).

The crystallographic *B*-factors of the 4 structures are at different levels (Table 1), which is probably due to differences in data collection, scaling, and resolution. The listed *B*-factor averages indicate that subunit II is always more rigid than subunit I, which is most likely a consequence of the slightly asymmetric crystal contacts discussed in detail by Mittl and Schulz (1994). Moreover, the prosthetic group FAD is generally the most rigid entity, whereas the bound coenzyme NAD(P) is relatively mobile.

Within the NAD(P) molecules, there exists an appreciable difference between the *B*-factors for the nicotinamide and the adenosine ends. In the Wild-type:NADP complex, the average *B*-factors of nicotinamide, ribose, pyrophosphate, ribose-phosphate, and adenine are 43, 42, 30, 17, and 23 $Å^2$, respectively. The corresponding values for the Mutant:NAD complex are 23, 23, 18, 15, and 11 $Å^2$. The nicotinamides were probably assigned high *B*-factors during the refinement procedure because they have less than full occupancies. It is likely that this is caused by partial oxidation of the enzyme and the applied NAD(P)H because $NAD(P)^+$ is known to bind to the oxidized enzyme only with its adenosine phosphate moiety (Karplus & Schulz, 1989). In both measurements (see below) we used crystals in capillaries filled with solutions of NADPH or NADH, which probably were oxidized to some extent during soaking and data collection. We estimate that the nicotinamide sites are occupied to 75% and more. The adenosine sites are fully occupied because the adenosine *B*-factors agree with those of the main chain. The effect was not pronounced enough and the data resolution not high enough to refine multiple conformations of the coenzymes.

Table 1. *Characteristics of the refined models*

	Wild-type:NADP[a]		Mutant:NAD[a]	
R-factor, %	20.8	(16.8)	16.9	(16.8)
Resolution range, Å	7–2.0	(7–1.86)	7–2.2	(7–1.74)
Unique reflections	56,997	(82,609)	42,272	(100,974)
Number of non-hydrogen atoms				
All atoms	7,487	(7,586)	7,425	(7,512)
Water molecules	450	(645)	410	(585)
RMS deviations from standard geometry				
Bond lengths, Å	0.015	(0.016)	0.015	(0.014)
Bond angles, deg	2.9	(2.8)	3.0	(2.7)
Average *B*-factors, $Å^2$				
Main chain, subunit I	18.9	(19.9)	14.6	(23.6)
Main chain, subunit II	16.5	(18.1)	13.5	(23.3)
Water molecules, total	34.0	(41.6)	28.8	(42.8)
Side chain, total	23.1	(28.1)	18.4	(34.5)
FAD, total	12.0	(12.5)	10.2	(17.0)
NAD(P), total	29.8		17.7	

[a] The numbers in parentheses refer to the respective unligated structures. The Wild-type structure data are from Mittl and Schulz (1994). All data are averages over both crystallographically independent subunits.

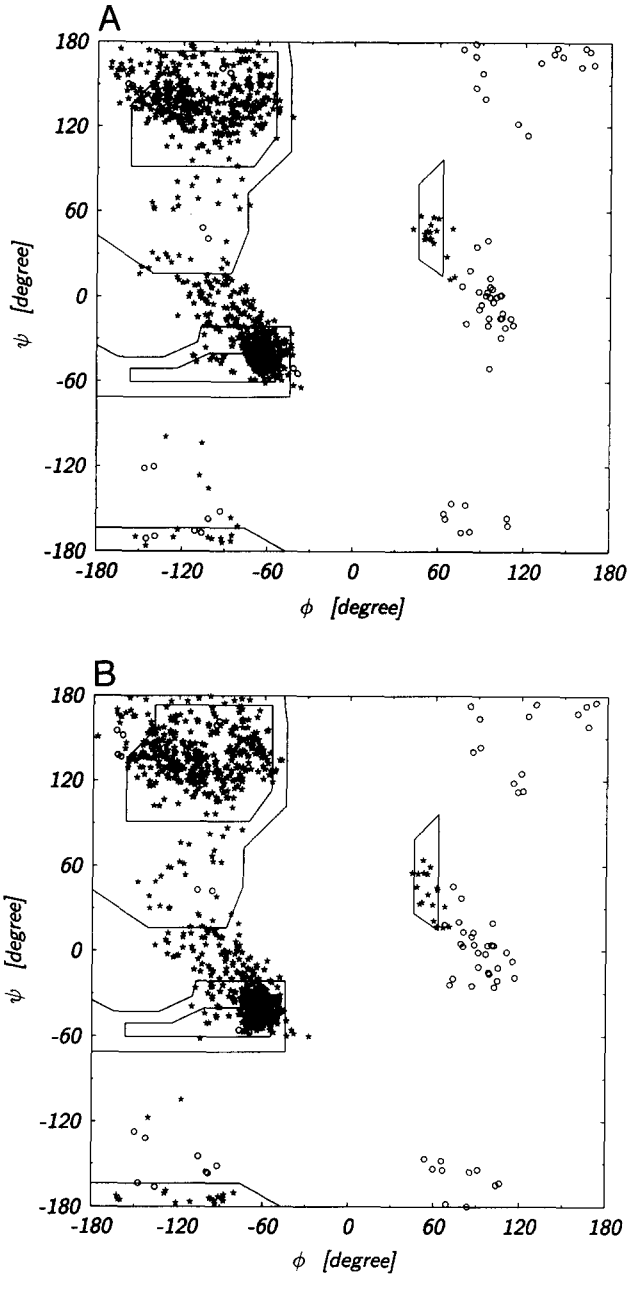

Fig. 1. Ramachandran plots of the ligated enzymes. Non-glycine residues are given by stars and glycines by open circles. **A:** Both subunits of complex Wild-type:NADP, the residues in unfavorable regions are Lys 36, around (−120°, −100°) and Lys 199, around (−105°, −130°). **B:** Both subunits of complex Mutant:NAD, the two Lys 36 near (−130°, −110°) are in an unfavorable region, whereas the two mutated Phe 199 around (−95°, −175°) are in a favorable region.

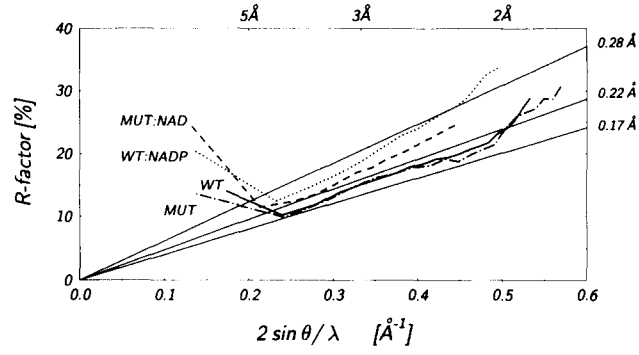

Fig. 2. Luzzati (1952) plot of the refined structures. The *R*-factor is given for Wild-type (——), complex Wild-type:NADP (· · ·), Mutant (— · — · —), and complex Mutant:NAD (— —). The theoretical lines of constant error are plotted for reference.

In all 4 models, the 2 subunits of the dimeric enzyme are crystallographically independent and therefore constitute 2 sets of structure data each. Here, we always consider both sets. Except for the unligated Mutant structure (see below, Fig. 3A), however, there is no subunit difference worth reporting.

In order to change the coenzyme specificity of GR_{eco} from NADP to NAD, 7 point mutations were made in each subunit (Scrutton et al., 1990; see Kinemages 1 and 2). These mutations are located close together; all C_α atoms (except for A183G at 11 Å) are within a distance of 7 Å from the central residue 197, which is close to the adenosine ribose. Because A183G is obviously of minor importance and has little or no effect on coenzyme specificity (Scrutton et al., 1990), we need not consider it further. The local concentration of the mutations is likely to disrupt the evolved structure of this region, giving rise to less well-defined features. A conformational heterogeneity in the mutated region is shown in Figure 3.

In the generally less well-defined subunit I (higher *B*-factors, Table 1) of the unligated Mutant structure, we find 2 conformations of the peptide connecting Gly 174 with Ala 175; the peptide assumes 2 opposite orientations, each with about half occupancy (Fig. 3A). In subunit II, the respective peptide conformation is unique and fixed by hydrogen bond 175-N· · ·Glu 197-OE1 to an obviously deprotonated glutamic acid (Fig. 3B). One of the 2 conformations of subunit I corresponds to subunit II; the other one is novel. The novel peptide orientation sets the side-chain conformation of Glu 197. Glu 197 is most likely protonated, donating a hydrogen bond to 174-O and accepting bonds from 198-N and 199-N (Fig. 3A). A protonated glutamate is compatible with the pH value of 5.5 during the measurement. The structural heterogeneity seems to be produced by half-protonation of Glu 197. The novel subunit I conformation is of minor importance because the alternative conformation (also found in subunit II, Fig. 3B) is assumed on NAD-binding in both subunits of the ligated Mutant. Accordingly, the novel conformation is unable to bind NAD, but can switch to the binding conformation. The observed heterogeneity in one of the subunits demonstrates that mutations may cause a "softening" of their environment.

Comparison of the unligated structures

In multidomain proteins like glutathione reductase, mutations may give rise to domain rearrangements. In order to investigate this possibility, we superimposed the complete dimers of the unligated Wild-type and Mutant enzymes. The superposition resulted in an RMS ΔC_α of 0.29 Å for 894 C_α atoms, which approaches the noise level and corresponds to the values of the internal comparisons between subunit I and II (see above). The

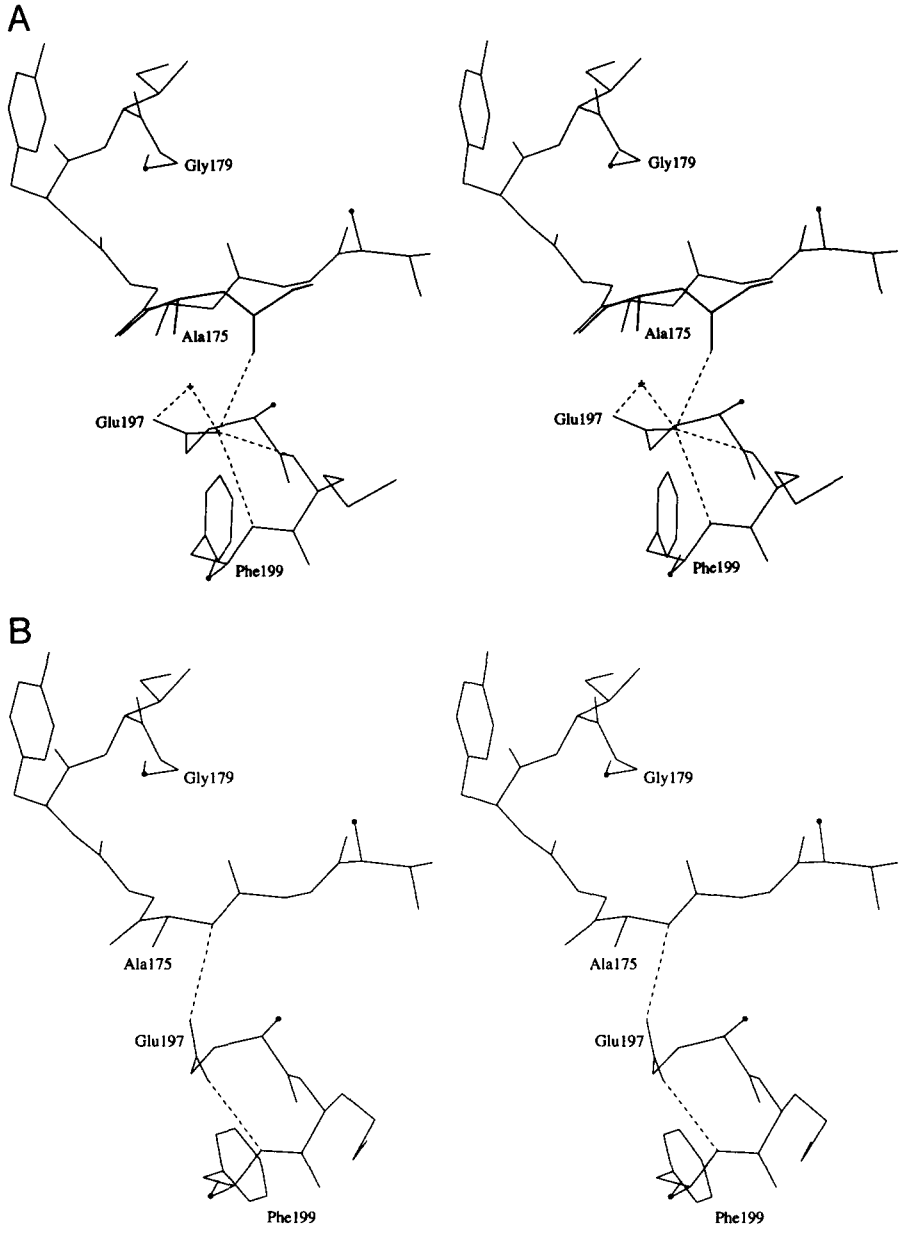

Fig. 3. Stereo view illustrating the conformational softness of the mutated region in the unligated Mutant structure. **A:** Subunit I harboring 2 approximately equally occupied conformations of Gly 174–Ala 175; the novel conformation (thick lines) corresponds to the fitted side chain of Glu 197 (see text); possible hydrogen bonds are indicated by dashed lines; Ala 175-O forms a good hydrogen bond to 193-N (not shown) and may have some secondary interactions with the carboxylate of Glu 197 and/or the depicted water molecule. **B:** The same view but with subunit II; this subunit has only 1 conformation.

relative positions of the domains were evidently undisturbed, allowing us to focus on the NADP domain, where the largest differences occurred (Kinemage 1).

After superimposing the NADP domains of the unligated structures, we observed residual chain deviations, which are plotted in Figure 4. This plot shows 4 peaks with C_α deviations above 0.5 Å, whereas the other values are around the noise level. The 2 largest peaks are direct consequences of the mutations (see below), whereas the other 2 peaks reflect secondary effects on neighboring main chains. Interestingly enough, the residues around the 2 smaller peaks are involved in crystal contact-V in the direction of the *b*-axis (Mittl & Schulz, 1994). In both Mutant crystals, the *b*-axis is shortened by 1 Å (see below, Table 5), which is probably a consequence of this main-chain displacement. Moreover, the crystal dimension is shortened in the *b* direction, giving rise to a platelike habit that contrasts with the more equal-dimensioned Wild-type crystals. Presumably, the mutations have reduced the strength of crystal contact-V, magnifying a microscopic change to a macroscopic difference.

A more direct version of the changes is depicted in Figure 5, where the mutated region of subunit II is superimposed on the Wild-type. For clarity, the changes may be described sequentially as: Ala 179 → Gly causes a 90° rotation of peptide 174–175 such that 175-N forms a hydrogen bond to the newly introduced carboxylate (Val 197 → Glu), which in turn connects to 199-N, attracting the chain segment around position 199 (second peak in Fig. 4). The segment around 199 then displaces the hydrogen bonded neighboring segment 226–229 (third peak in Fig. 4), which in turn displaces its hydrogen bonded neighbors 247–249 (fourth peak in Fig. 4; see also below, Fig. 6). In reality, the 2 mutations are coupled and neither of them can be taken as initiation point.

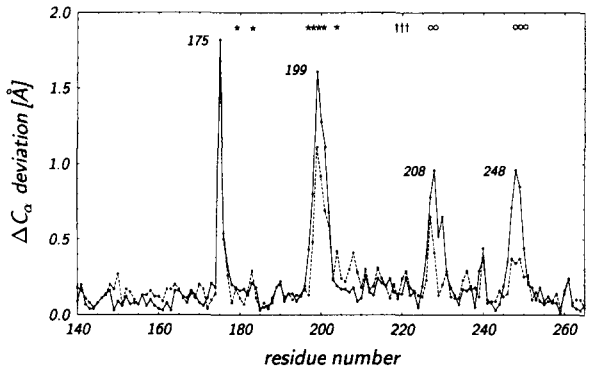

Fig. 4. Residual distances between the C_α atoms of the NADP-domains of GR_{eco} Wild-type and Mutant after a best superposition of these domains based on the 119 C_α atoms with deviations below 0.5 Å. The plots are given for subunit I (solid lines) and for subunit II (broken lines). The positions of the 7 point mutations are indicated by stars. The residues of crystal contact-Ia (only in subunit I; see Mittl & Schulz, 1994) are marked by daggers and those in crystal contact-V (both subunits) by circles.

Figure 5 shows that the exchanges Arg 198 → Met, Lys 199 → Phe, and Arg 204 → Pro render the environment of Glu 197 rather nonpolar, increasing its hydrogen bonding strength appreciably (Fersht et al., 1985). The carboxylate of Glu 197 is poised to bind the adenosine ribose tightly. The exchange His 200 → Asp should be of minor importance because this side chain points toward the solvent and away from the binding site.

Structural changes on coenzyme binding

As indicated by the heterogeneity at peptide 174–175 (Fig. 3A), which disappeared on NAD-binding, the 7 mutations did not quite suffice to form a binding site that was stable by itself, but the design came close enough to enable NAD to enforce the correct binding structure. In order to analyze the solidification of the NAD site in more detail, we determined the *B*-factor changes on coenzyme binding. Because the *B*-factors obviously varied with data collection, scaling, and resolution (Table 1), we always subtracted the respective overall average *B*-factors before calculating the differences.

The results in Figure 6 demonstrate that the side chains of the mutated segment 197–204 are mobile in the unligated state, but freeze out on coenzyme binding. A closer look shows that there is an appreciable solidifying of the Mutant's glutamate at residue position 197, but almost no effect for the Wild-type's valine at the same position. Moreover, the Mutant's Met 198 and Phe 199 solidify more strongly than the Wild-type's Arg 198 and Lys 199. With respect to His 200 → Asp, the side chain of which points away from the adenosine, both structures behave similarly. The larger effect for Arg 204 (Wild-type) as compared with Pro 204 (Mutant) is probably caused by the different side-chain lengths. The peak at position 192 is spurious because it involves a very mobile lysine at the protein surface far away from the binding sites, the environment of which remained constant. The peaks at 176–177 merely reflect inaccuracies at Tyr 177 that are discussed below.

For the main chains, the effect of coenzyme binding is less pronounced. In both structures, however, the main chain of segment 197–204 solidifies, and the effect is stronger for the Mutant. Interestingly enough, the Ramachandran plot in Figure 1 shows that Wild-type's Lys 199 (like the equivalent residue of *human* glutathione reductase; Karplus & Schulz, 1987) has unfavorable (ϕ, ψ) angles, whereas Mutant's Phe 199 has not. Obviously, the mutation had softened the structure such that the strained main chain was relaxed. In conclusion, coenzyme binding causes a chain solidification in the Mutant and also in the Wild-type. The Mutant shows a larger difference, probably because its starting structure is softer.

The motion of Tyr 177 as an induced fit on NADP-binding is already known from the *human* enzyme (Karplus & Schulz, 1989). Tyr 177 moves such that its side chain presses the incoming nicotinamide onto the isoalloxazine of FAD. In our X-ray analyses of the ligated structures, the Tyr 177 region is less accurate than the rest of the structure because we encountered incomplete Tyr displacement caused by incomplete occupation of the nicotinamide site as described above. We therefore refrain from analyzing the changes around position 177 in Figure 6.

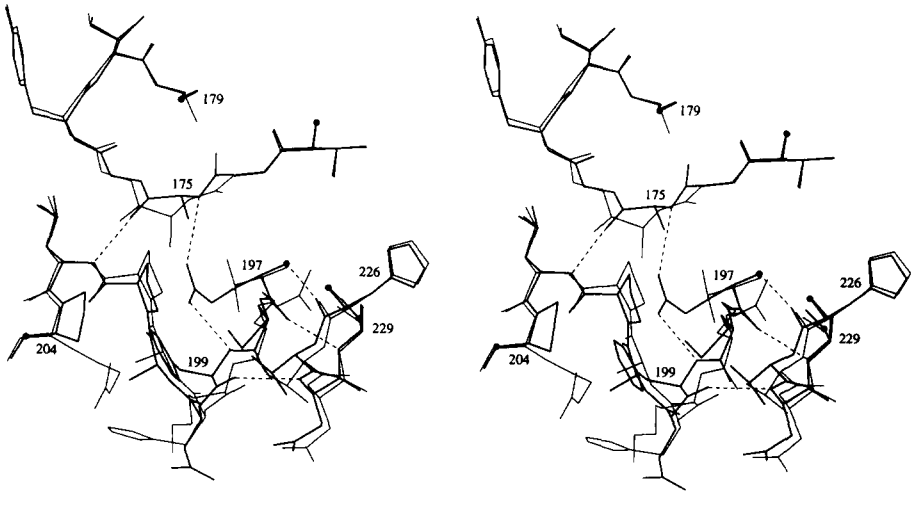

Fig. 5. Stereo view of structural difference in the mutated region. The superposition is identical to Figure 4. Shown are 3 chain segments (residues 173–179, 197–204, and 226–229 of subunit II) of GR_{eco} Wild-type (thin lines) and Mutant (thick lines) that contain 6 of the 7 exchanges. Six important hydrogen bonds of the Mutant are given (dashed lines). The chain cuts of the Mutant structure are marked by dots.

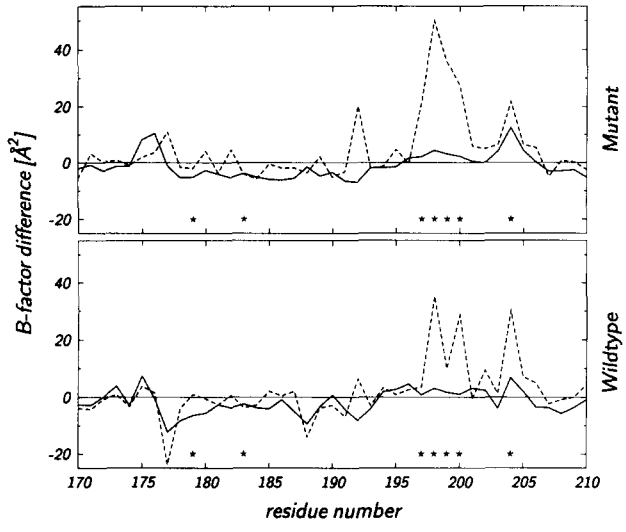

Fig. 6. Mobility changes on NAD(P)-binding in GR_{eco} Wild-type and Mutant. The *B*-factor differences of the main chains (thick lines) and the side chains (dashed lines) are averaged over both subunits. In all cases, the overall *B*-factor averages have been subtracted in order to compensate for differences in data collection, scaling, and resolution. The plotted value for residue *i* equals B_i(Mutant) − $B_{average}$(Mutant) − B_i(Mutant:NAD) + $B_{average}$(Mutant:NAD), where all *B* denote values averaged over subunits I and II and the B_i refer to the mean *B*-factors of side- or main-chain atoms, respectively. The same formula was applied for the Wild-type. The point mutations are marked by stars.

Differences between the ligated structures

A chain fold superposition of the ligated NAD(P) domains is shown in Figure 7. It illustrates the binding-site contraction in the Mutant caused by the introduction of Gly 179 and Glu 197, which is transferred to crystal contact-V at positions 248–250, causing the crystal change discussed above. The binding mode differences between NAD and NADP are small. The dinucleotide conformations are well retained, as demonstrated by the torsion angles (Table 2). The largest change occurs at the adenosine ribose, where the pucker has become 2′*endo* in the Mutant. Figure 7 shows an overall shift of NAD when compared with NADP. The adenosine of NAD is drawn by about 1 Å toward the protein, although its binding site has contracted in the Mutant (Fig. 4). This shift becomes progressively smaller toward the nicotinamide but may still hinder the transfer of reduction equivalents from nicotinamide to isoalloxazine and thus, catalysis, by elongating the distance.

Details of the coenzyme-binding differences are given in Table 3, which lists the hydrogen bonds to the protein and to buried water molecules. The interactions of NAD and NADP resemble each other closely in their nicotinamide moieties but differ completely for the adenosine moieties, as also illustrated in Figure 8 and Kinemage 2. In the Wild-type:NADP complex, the 2′-phosphate is held by tight hydrogen bonds to Arg 198 and Arg 204 such that the guanidinium group of Arg 198 forms a sandwich with the adenine as found with other adenine sites, e.g., the adenine of ATP in adenylate kinases (Müller & Schulz, 1992). The only hydrogen bond of adenine is between N3A and a buried water molecule. The ribose ring oxygen O4′A forms a rather long hydrogen bond with 175-N (Fig. 8; Table 3), which is presumably weak due to the low polarity of this oxygen. This interaction has been emphasized by Baker et al. (1992), but we consider it less important. The 3′-hydroxyl does not interact with the protein.

In contrast with its minor role in NADP binding, the adenosine ribose is most important for the recognition of NAD. There are 2 strong hydrogen bonds between its 2′- and 3′-hydroxyls and the carboxylate of Glu 197, which forms 2 further hydrogen bonds to the backbone (here to 175-N and 199-N, Fig. 9). Given the 2′*endo* pucker of the ribose, these 4 hydrogen bonds are in very favorable geometry. They most probably provide the largest contribution to NAD binding.

A superimposition of Mutant:NAD with NAD bound to lactate dehydrogenase and to NADH peroxidase is depicted in Figure 9, showing that the 4 hydrogen bonds constitute a typical scheme for NAD-binding to a Rossmann fold. The adenosine riboses are in close proximity and all of them form the 4-H-bond scheme with the carboxylate. The side chains at 198 and 199 (GR_{eco} numbers) are all nonpolar, increasing the bond strengths by fending off water.

The GR_{eco} structures underline the importance of the sequence fingerprint for NAD(P) binding: Gly^1-x^2-Gly^3-x^4-x^5-Gly^6(Ala^6). With Gly^6, this fingerprint was reported for NAD sites (Wierenga et al., 1986), whereas Ala^6 is more common for

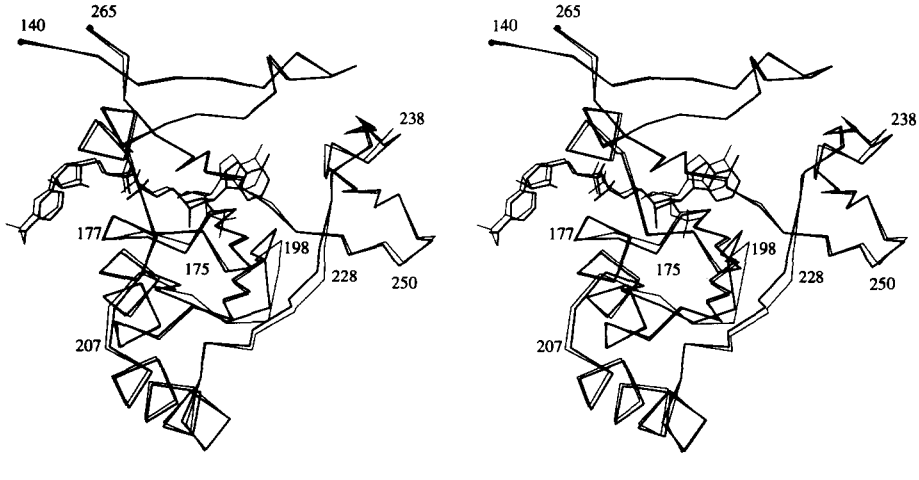

Fig. 7. Stereo view of the general changes of the binding mode of NAD(P) between GR_{eco} Wild-type (thin lines) and Mutant (thick lines). The superposition is identical to Figure 4 except that the ligated structures are used instead of the unligated ones. The coenzymes and the C_α chain folds of subunit II are depicted. Some residues are labeled.

Table 2. *Dihedral angles of bound NAD(P)*

Torsion angle[a]	Angle definition[a]	NADP[b], deg	NAD[b], deg
χ_A	C4A-N9A-C1'A-C2'A	138 (137)	147 (148)
A-ribose	Pucker	3'*endo*	2'*endo*
ξ_A	C3'A-C4'A-C5'A-O5'A	−89 (−81)	−76 (−84)
χ'_A	C2'A-O2'A-PR-O2PR	65 (58)	–
θ'_A	C1'A-C2'A-O2'A-PR	90 (92)	–
θ_A	C4'A-C5'A-O5'A-PA	141 (148)	165 (149)
ψ_A	C5'A-O5'A-PA-OAN	59 (50)	61 (76)
ϕ_A	O5'A-PA-OAN-PN	78 (85)	92 (66)
ϕ_N	O5'N-PN-OAN-PA	101 (75)	80 (97)
ψ_N	C5'N-O5'N-PN-OAN	12 (58)	47 (50)
θ_N	C4'N-C5'N-O5'N-PN	−138 (−167)	−161 (−164)
ξ_N	C3'N-C4'N-C5'N-O5'N	60 (43)	56 (44)
N-ribose	Pucker	3'*endo*	3'*endo*
χ_N	C2N-N1N-C1'N-C2'N	70 (68)	69 (60)

[a] The nomenclature follows Pai et al. (1988) and Karplus and Schulz (1989).
[b] The numbers are for subunit I; those in parentheses specify the angles in subunit II. The subunits are defined by their centers of gravity in Å, which are (19, 15, −1) for subunit I and (41, −14, 1) for subunit II.

NADP sites (Hanukoglu & Gutfinger, 1989). In GR_{eco}, the exchange $Ala^6 \rightarrow Gly^6$ at position 179 had a profound effect (Mittl et al., 1993) because it allowed a 90° rotation of peptide Gly^1-x^2, creating the important interaction 175-N···Glu 197-OE1 of the typical 4-H-bond scheme for the 2'*endo* puckered ribose (Fig. 9). Furthermore, it rotates the x^2 side chain into the protein interior (Fig. 8), which would otherwise collide with the 3'-hydroxyl of the ribose. This peptide bond rotation has also been detected in glutamate dehydrogenase (Baker et al., 1992) and dihydrolipoamide dehydrogenase (Mattevi et al., 1992) when comparing native structures.

Table 3. *Hydrogen bonds between NAD(P) and protein*

NAD(P) atom	Wild-type:NADP		Mutant:NAD	
	Atom[a]	Distance,[b] Å	Atom[a]	Distance,[b] Å
N7N	Val 342-O	3.0 (2.6)	Val 342-O	2.9 (2.8)
	Glu 181-OE1	3.3 (3.9)	Glu 181-OE1	3.2 (3.1)
O7N	Wat 115 (28)	2.7 (2.6)	Wat 20 (106)	2.8 (2.7)
O2'N	Glu 309-O	2.9 (2.8)	Glu 309-O	2.8 (2.8)
O3'N[c]	NADP-O1A	3.1 (3.3)	NAD-O1A	3.6 (3.2)
O4'N	Wat 250 (379)	3.2 (3.1)	Wat 109 (171)	3.1 (3.2)
O1N	Ile 178-N	3.3 (3.1)	Ile 178-N	2.9 (3.0)
			Tyr 177-N	3.5 (3.4)
	Wat 70 (170)	2.9 (2.6)	Wat 87 (45)	2.8 (2.8)
O2N	Wat 35 (17)	2.6 (2.8)	Wat 150 (79)	2.9 (3.0)
	Gly 262-N	3.3 (3.5)	Gly 262-N	3.1 (3.2)
O2'A			Glu 197-OE1	2.7 (2.7)
O3'A			Glu 197-OE2	2.5 (2.6)
O4'A	Ala 175-N	3.1 (3.5)		
O1PR	Arg 204-NH1	2.8 (2.9)		
	Wat 64 (38)	2.8 (2.7)		
O2PR	Arg 204-NH1	2.9 (3.2)		
	Arg 198-NH2	3.3 (2.9)		
O3PR	Arg 198-NE	2.9 (2.9)		
	Wat 141 (22)	2.7 (2.7)		
N3A	Wat 141 (22)	2.9 (2.7)	Met 198-N	3.3 (3.4)

[a] The water molecule numbers refer to subunit I; those in parentheses are from subunit II. All listed water molecules are buried on NAD(P) binding and form at least 1 hydrogen bond to a polypeptide atom.
[b] All distances refer to subunit I; those in parentheses are from subunit II.
[c] Hydrogen bond within NAD(P).

Conformations of fingerprint residues and riboses in the Wild-type and Mutant GR_{eco} structures are given in Table 4, together with those of other structures refined to high resolution. A grouping according to Gly^6 and Ala^6 shows a distinct conformational difference in residues Gly^1-x^2. This grouping applies also for the ribose pucker and for NAD versus NADP binding. The NADP sites contain Ala^6 and no carboxylate, showing specific torsion angles that describe one of the orientations of peptide Gly^1-x^2. In this orientation, the x^2 side chain enforces a 3'*endo* puckered ribose and the x^2 peptide nitrogen interacts weakly with the ring oxygen O4'A. In contrast, the NAD sites have Gly^6 together with a carboxylate, and peptide Gly^1-x^2 assumes the other orientation that allows for the 4-H-bond scheme binding 2'*endo* puckered ribose (Fig. 9). Thus, Table 4 defines 2 distinct types of NAD(P)-binding sites containing the fingerprint. It should be noted that there may be further types. Also, there exist a number of NAD(P)-binding enzymes lacking a Rossmann fold and its sequence fingerprint (Schulz, 1992).

Conclusion

The high-resolution structures of unligated and ligated Wild-type and Mutant forms of GR_{eco} explain the specificity change from NADP to NAD with rather small structural changes. They also indicate the difficulties that arise in trying to engineer binding sites. A remaining problem is the relatively low catalytic activity of the engineered Mutant (k_{cat}/K_m for NADH = 24.4 μM^{-1} min^{-1}; Scrutton et al., 1990), which did not reach the wild-type level (740 μM^{-1} min^{-1} for NADPH) although all the amino acid exchanges are far away from the reactive C4 atom of the

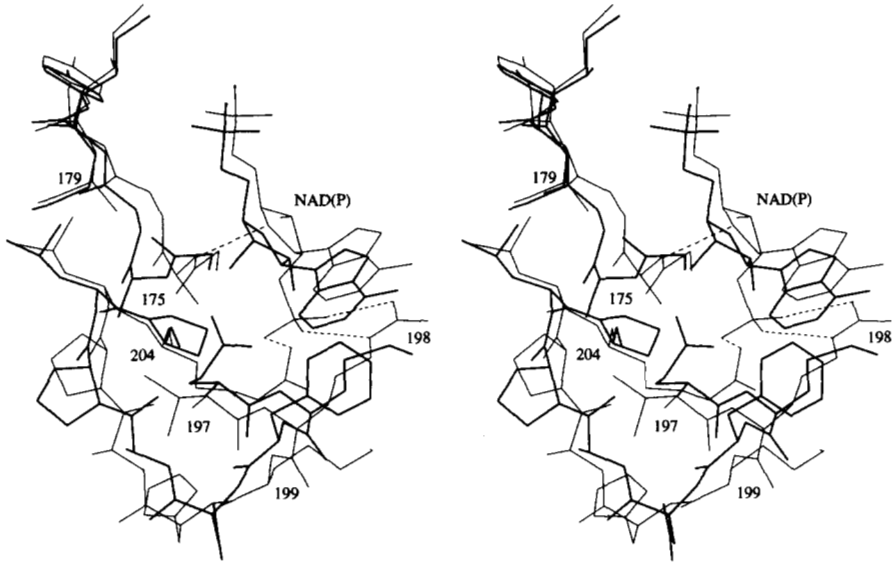

Fig. 8. Stereo view showing the differences of the NAD(P)-binding modes in GR_{eco} Wild-type (thin lines) and Mutant (thick lines). Depicted are the sequence fingerprint residues 174–179 and the mutated segment 197–204 of subunit I, together with the adenosine moiety of NAD(P). Some hydrogen bonds of the Wild-type:NADP complex are given as dashed lines.

nicotinamide ring. An explanation may be indicated in Figure 7, showing a slight retraction of the nicotinamide from the isoalloxazine, which could impede the electron transfer. This shift is caused by the adenosine being drawn closer to the protein. Such a shift can only be compensated by a long-range structural change, which will be difficult to design in a rational manner.

Materials and methods

Purification and crystallization

Wild-type GR_{eco} was purified and crystallized as described earlier (Scrutton et al., 1987; Mittl & Schulz, 1994). The NAD-dependent Mutant (mutations A179G, A183G, V197E, R198M, K199F, H200D, and R204P) of Scrutton et al. (1990) was produced and purified in a manner similar to that of the Wild-type, except that the final 2′,5′-ADP-Sepharose-4B affinity chromatography was not applicable. For this last step, 35 mg of enzyme was loaded onto a phenyl-Sepharose column (1 × 15 cm) equilibrated with 20 mM potassium phosphate buffer, pH 7.5, containing 1.05 M ammonium sulfate. The column with bound enzyme was washed with 150 mL of the same buffer and then eluted with 100 mL of buffer with lower ammonium sulfate concentration (0.85 M). A subsequent ultrafiltration brought the enzyme concentration to 30 mg/mL. The Mutant was pure as judged by SDS-polyacrylamide electrophoresis and isoelectric focusing; it was crystallized under the same conditions as the Wild-type (Mittl & Schulz, 1994).

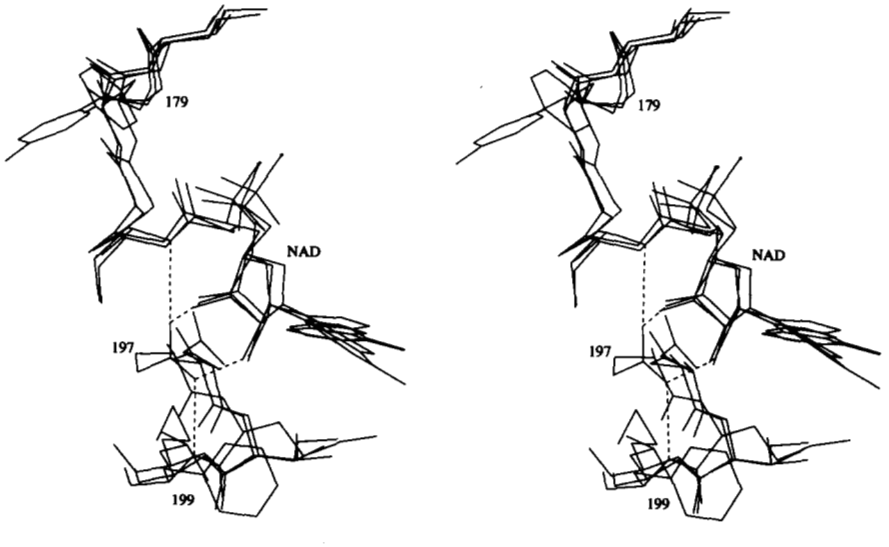

Fig. 9. The crucial part of the binding structure for NAD in GR_{eco} Mutant, in lactate dehydrogenase (Abad-Zapatero et al., 1987), and in NADH peroxidase (Stehle et al., 1993). The superposition is based on equivalent residues of the first $\beta\alpha\beta$-unit of the Rossmann fold for NAD binding (residues 169–191 and 193–200 of subunit II of GR_{eco} Mutant; residues 22–44 and 48–55 of lactate dehydrogenase; residues 151–173 and 175–182 of NADH peroxidase). The sequence fingerprint residues Gly^1-x^2-Gly^3-x^4-x^5-Gly^6 for NAD binding are depicted together with the adenosine moiety of NAD (cut marked by a dot) and the 3-residue segment Glu 197-Met-Phe of GR_{eco} Mutant (Asp-Val-Met in lactate dehydrogenase; Asp-Ile-Leu in NADH peroxidase). The 4 essential hydrogen bonds of GR_{eco} Mutant are drawn as dashed lines. Glu 197 of the GR_{eco} Mutant forms hydrogen bonds only to 175-N and 199-N of the polypeptide, whereas the shorter (equivalent) aspartates of the other 2 enzymes have an additional interaction with the peptide nitrogens equivalent to 198-N.

Table 4. *Conformations of fingerprint residues and NAD(P)*

Enzyme[a]	Coenzyme	Adenosine ribose pucker	Gly[1]		x[2]		
			ϕ, deg	ψ, deg	Residue	ϕ, deg	ψ, deg
Containing Gly[6]							
GR_{eco} Mutant[b]	NAD	2′*endo*	120	116	Ala 175	−116	57
Lactate dehyd.[c]	NAD	2′*endo*	119	107	Val 28	−108	60
Dihydrolip. dehyd.[d]	NAD	2′*endo*	118	124	Ala 188	−109	46
NADH-peroxidase[e]	NAD	2′*endo*	117	126	Ser 157	−116	49
Average			119	118		−112	53
Containing Ala[6]							
GR_{eco} Wild-type[b]	NADP	3′*endo*	143	171	Ala 175	−150	18
GR_{hum}[f]	NADP	3′*endo*	137	164	Ala 195	−134	19
Thioredoxin red.[g]	NADP	–	152	169	Gly 153	−134	2
Trypanothione red.[h]	NADP	–	140	154	Gly 195	−106	−3
Average			143	165		−131	9

[a] Only structures with better than 2.5-Å resolutions are considered. There exists a medium-resolution structure of an NADP-dependent mercuric ion reductase containing Gly[6] (Schiering et al., 1991), which shows a 2′*endo* puckered ribose. If this feature were confirmed at high resolution, it would corroborate the grouping of this table insofar as Gly[6] determines the ribose pucker, but it would break the convention that Gly[6] normally goes with NAD.

[b] The individual (ϕ, ψ) angles of the subunits have been averaged. The deviations are in the range of 3°.

[c] Lactate dehydrogenase (Abad-Zapatero et al., 1987).

[d] Dihydrolipoamide dehydrogenase from *Azotobacter vinelandii* (Mattevi et al., 1991); the NAD pucker is from the *Pseudomonas putida* enzyme (Mattevi et al., 1992).

[e] NADH-peroxidase (Stehle et al., 1993).

[f] Human glutathione reductase (Karplus & Schulz, 1989).

[g] Thioredoxin reductase (Kuriyan et al., 1991b).

[h] Trypanothione reductase (Kuriyan et al., 1991a).

Wild-type and Mutant crystals are isomorphous and belong to space group $P2_1$, with 2 subunits per asymmetric unit (Table 5). However, the Mutant crystals have a 1 Å shorter *b*-axis. The Wild-type crystals grew to dimensions of 1,000 × 600 × 250 μm^3, whereas the Mutant crystals were thinner, reaching a size of 2,000 × 80 × 1,000 μm^3. The enzyme:coenzyme complexes were prepared by soaking the crystals in solutions of the reduced coenzyme dissolved in 100 mM potassium phosphate buffer, pH 5.5, with 20% PEG-8000. Details are given in Table 5.

Data collection

Because the complexes between enzyme and NAD(P)H were sensitive to air oxidation, the crystals were fixed with Sephadex

Table 5. *Statistics of data collection*

Enzyme	Soak[a]	Time, days	Cell parameters[b] Δa, Å	Δb, Å	Δc, Å	$\Delta\gamma$, deg	R_{sym},[c] %	R_{nat},[d] %	Resolution limit, Å	Completeness Total, %	Outermost shell, %
Wild-type	–	–	–	–	–	–	9.1	–	1.86	95.1	78 (1.89–1.86 Å)
Wild-type[e]	10 mM NADPH	3	0.0	+0.4	+0.3	−0.5	10.2	25.1	2.00	81.7	50 (2.07–2.00 Å)
Mutant[f]	–	–	−0.5	−0.8	+0.5	−0.2	6.8	24.5	1.74	94.0	93 (1.78–1.74 Å)
Mutant	10 mM NADH	2	0.0	−1.1	+0.3	−0.2	8.7	32.6	2.20	82.2	65 (2.28–2.20 Å)

[a] The soaking buffer was 100 mM potassium phosphate, pH 5.5, 20% PEG-8000, 0.02% NaN_3 and NAD(P)H as specified.

[b] Cell parameter changes in relation to Wild-type crystals (a = 120.5 Å, b = 73.6 Å, c = 60.5 Å, γ = 83.0°).

[c] $R_{sym} = \Sigma_{i,\boldsymbol{h}} |I(i,\boldsymbol{h}) - \langle I(\boldsymbol{h})\rangle| / \Sigma_{i,\boldsymbol{h}} I(i,\boldsymbol{h})$, where $\boldsymbol{h} = hkl$, i = symmetry-related reflections, and I = intensity.

[d] $R_{nat} = 2\Sigma_{\boldsymbol{h}} |F_1(\boldsymbol{h}) - k * F_2(\boldsymbol{h})| / \Sigma_{\boldsymbol{h}} [F_1(\boldsymbol{h}) + F_2(\boldsymbol{h})]$, where $k = \Sigma_{\boldsymbol{h}} F_1(\boldsymbol{h}) / \Sigma_{\boldsymbol{h}} F_2(\boldsymbol{h})$, $\boldsymbol{h} = hkl$ and F = structure factor amplitude; set $F_2(\boldsymbol{h})$ was always Wild-type.

[e] In another measurement to 2 Å resolution with a 7-day soak of 30 mM NADH, no bound NAD could be detected, although the enzyme was at least partially reduced at the redoxactive disulfide. The respective structure has therefore not been refined.

[f] This data set was merged from synchrotron data and a 2.0-Å-resolution data set from the area detector (see text).

G-25 in capillaries filled with the soaking solution. The filling increased the X-ray background and the X-ray absorption, limiting the resolution of data collection. Note that it is not clear yet whether the coenzyme binds in the crystals as $NAD(P)^+$ at the 2-electron-reduced enzyme (open redoxactive disulfide) in a complex poised for GSSG reduction, or as NAD(P)H, forming a 4-electron-reduced complex.

X-ray data were collected on a 3-circle area detector (model X1000, Xentronics/Siemens) using CuKα radiation from a rotating anode generator (model RU200B, Rigaku) equipped with a graphite monochromator. The detector-to-crystal distance was 12 cm, each frame covered an angular range of 0.25° over a time of 120 s. The data were processed with program XDS (Kabsch, 1988). One crystal of the unligated Mutant was used to collect a 1.74-Å resolution data set with synchrotron radiation (λ = 1.01 Å, beam-line X11 at EMBL outstation, DESY). The resulting data were reduced with program MOSFLM/IMAGES and merged with a 2.0-Å resolution data set recorded with the area detector (Table 5).

Model building and refinement

The structure of Wild-type GR_{eco} had been refined to an *R*-factor of 16.8% at 1.86 Å resolution (Mittl & Schulz, 1994). This structure served as a starting point for establishing the structures of the Mutant and the 2 enzyme:coenzyme complexes. The Mutant was derived from a $(F_{obs} - F_{calc})\exp(i\alpha_{calc})$ and a $(2F_{obs} - F_{calc})\exp(i\alpha_{calc})$ electron density map. Strong difference densities were found around positions 174–176 and 179 as a consequence of the exchanges A179G and A183G. Weaker differences occurred in loop 197–204, which accommodates the 5 exchanges V197E, R198M, K199F, H200D, and R204P. The new residues were incorporated and the model was subjected to energy minimization at 3 Å resolution using program XPLOR (Brünger et al., 1987). After extending the resolution to 2 Å, the 300 strongest water molecules of the Wild-type structure were examined. They were included if they had densities above 3σ in an $(F_{obs} - F_{calc})$ map and deleted when the densities dropped below 1σ in the $(2F_{obs} - F_{calc})$ map. After extending the resolution to 1.74 Å, the peptide between Gly 174 and Ala 175 in subunit I showed density for 2 alternative conformations with about equal occupancies (Fig. 3A). In subunit II, this peptide assumed only 1 conformation.

The analyses of the 2 enzyme:coenzyme complexes started from the respective unligated structures. The strongest peaks (6σ) in the $(F_{obs} - F_{calc})$ maps occurred at the pyrophosphates of NAD(P) and at the 2′-phosphate (in the Wild-type:NADP complex). Both adenosine moieties of NAD(P) were well defined at contour levels of 2.5σ, whereas the nicotinamide moieties were weaker.

In the Wild-type:NADP complex, the distribution of positive and negative $(F_{obs} - F_{calc})$ densities around the nicotinamide indicated an induced fit as observed with human glutathione reductase (Karplus & Schulz, 1989). After rearranging Tyr 177 in a way similar to the human enzyme with its equivalent tyrosine, the bound nicotinamide and the surrounding polypeptide could be refined in good density. The nicotinamide ring had also relatively weak density in the $(F_{obs} - F_{calc})$ map of the Mutant:NAD complex. Again this problem was rectified by displacing the Tyr 177 side chain in the same way as in the Wild-type:NADP complex. Data on the refined structures are given in Table 1.

Acknowledgments

We thank Dr. J. Kuriyan for sending us the coordinates of trypanothione reductase and thioredoxin reductase prior to deposition in the Brookhaven Protein Data Bank and Dr. K.S. Wilson and his team for help with data collection at the EMBL outstation, Hamburg. The work was supported by the Land Baden-Württemberg, the Science and Engineering Research Council, and an ACE Award from CIBA-Geigy. A.B. was a Royal Society 1983 University Research Fellow. N.S.S. was a Research Fellow of the Royal Commission for the Exhibition of 1851. All coordinates and structure factors are deposited in the Protein Data Bank at Brookhaven, New York.

References

Abad-Zapatero C, Griffith JR, Sussmann JL, Rossmann MG. 1987. Refined crystal structure of dogfish lactate dehydrogenase. *J Mol Biol 198*: 445–467.

Baker PJ, Britton KL, Rice DW, Rob A, Stillman TJ. 1992. Structural consequence of sequence patterns in the fingerprint region of the nucleotide binding fold. *J Mol Biol 228*:662–671.

Bocanegra JA, Scrutton NS, Perham RN. 1993. Creation of an NADP-dependent pyruvate dehydrogenase multienzyme complex by protein engineering. *Biochemistry 32*:2737–2740.

Brünger AT, Kuriyan J, Karplus M. 1987. Crystallographic *R*-factor refinement by molecular dynamics. *Science 235*:458–460.

Fersht AR, Ski JP, Knill-Jones J, Lowe DM, Wilkinson AJ, Blow DM, Brick P, Carter P, Waye MMY, Winter G. 1985. Hydrogen bonding and biological specificity analysed by protein engineering. *Nature (Lond) 314*:235–238.

Hanukoglu I, Gutfinger T. 1989. cDNA sequence of adrenodoxin reductase, identification of NADP-binding sites in oxidoreductases. *Eur J Biochem 180*:479–484.

Kabsch W. 1988. Evaluation of single-crystal X-ray diffraction data from a position-sensitive detector. *J Appl Crystallogr 21*:916–924.

Karplus PA, Schulz GE. 1987. Refined structure of glutathione reductase at 1.54 Å resolution. *J Mol Biol 195*:701–729.

Karplus PA, Schulz GE. 1989. Substrate binding and catalysis by glutathione reductase as derived from refined enzyme:substrate crystal structures at 2 Å resolution. *J Mol Biol 210*:163–180.

Kuriyan J, Kong XP, Krishna TSR, Sweet RM, Murgolo NJ, Field H, Cerami A, Henderson GB. 1991a. X-ray structure of trypanothione reductase from *Crithidia fasciculata* at 2.4 Å resolution. *Proc Natl Acad Sci USA 88*:6764–6768.

Kuriyan J, Krishna TSR, Wong L, Guenther B, Pahler A, Williams CH Jr, Model P. 1991b. Convergent evolution of similar function in two structurally divergent enzymes. *Nature(Lond) 352*:172–174.

Luzzati V. 1952. Traitement statistique des erreurs dans la détermination des structures cristallines. *Acta Crystallogr 5*:802–810.

Mattevi A, Oblomova G, Sokatch JR, Betzel C, Hol WGJ. 1992. The refined crystal structure of *Pseudomonas putida* lipoamide dehydrogenase complex with NAD^+ at 2.45 Å resolution. *Proteins Struct Funct Genet 13*:335–351.

Mattevi A, Schierbeek AJ, Hol WGJ. 1991. Refined crystal structure of lipoamide dehydrogenase from *Azotobacter vinelandii* at 2.2 Å resolution. *J Mol Biol 220*:975–994.

Mittl PRE, Berry A, Scrutton NS, Perham RN, Schulz GE. 1993. Structural differences between wild-type NADP-dependent glutathione reductase from *Escherichia coli* and a redesigned NAD-dependent mutant. *J Mol Biol 231*:191–195.

Mittl PRE, Schulz GE. 1994. The structure of glutathione reductase from *Escherichia coli* at 1.86 Å resolution. *Protein Sci 3*:799–809.

Müller CW, Schulz GE. 1992. Structure of the complex between adenylate kinase from *Escherichia coli* and the inhibitor Ap_5A refined at 1.9 Å resolution. *J Mol Biol 224*:159–177.

Pai EF, Karplus PA, Schulz GE. 1988. Crystallographic analysis of the binding of NADPH, NADPH fragments, and NADPH analogues to glutathione reductase. *Biochemistry 27*:4465–4474.

Rescigno M, Perham RN. 1994. Structure of the NADPH-binding motif of glutathione reductase: Efficiency determined by evolution. *Biochemistry 33*:5721–5727.

Schiering N, Kabsch W, Moore MJ, Distefano MD, Walsh CT, Pai EF. 1991. Structure of the detoxification catalyst mercuric ion reductase from *Bacillus* sp. strain RC607. *Nature (Lond) 352*:168–171.

Schulz GE. 1992. Binding of nucleotides by proteins. *Curr Opin Struct Biol 2*:61–67.
Scrutton NS, Berry A, Perham RN. 1987. Purification and characterization of glutathione reductase encoded by a cloned and over-expressed gene in *Escherichia coli*. *Biochem J 245*:875–880.
Scrutton NS, Berry A, Perham RN. 1990. Redesign of the coenzyme specificity of a dehydrogenase by protein engineering. *Nature (Lond) 343*:38–43.
Stehle T, Claiborne A, Schulz GE. 1993. NADH binding site and catalysis of NADH-peroxidase. *Eur J Biochem 211*:221–226.
Stephens PE, Lewis HM, Darlison MG, Guest JR. 1983. Nucleotide sequence of the lipoamide dehydrogenase gene of *Escherichia coli* K12. *Eur J Biochem 135*:519–527.
Wierenga RK, Terpstra P, Hol WGJ. 1986. Prediction of the occurrence of the ADP-binding $\beta\alpha\beta$-fold in proteins, using an amino acid sequence fingerprint. *J Mol Biol 187*:101–107.

Forthcoming Papers

A quantitative methodology for the de novo design of proteins

S.E. Brenner and A. Berry

Solution structure of the DNA-binding domain of the heat shock transcription factor determined by multidimensional heteronuclear magnetic resonance spectroscopy

F.F. Damberger, J.G. Pelton, C.J. Harrison, H.C.M. Nelson, and D.E. Wemmer

Discovering structural correlations in α-helices

T.M. Klingler and D.L. Brutlag

On the evolution of alternate core packing in eightfold β/α barrels

A.R.C. Raine, N.S. Scrutton, and F.S. Mathews

Sequence determinants of the capping box, a stabilizing motif at the N-termini of α-helices

J.W. Seale, R. Srinivasan, and G.D. Rose

Formation of a native-like subdomain in a partially folded intermediate of bovine pancreatic trypsin inhibitor

J.P. Staley and P.S. Kim

Probing the catalytic roles of n_2-site glutamate residues in *Escherichia coli* glutamine synthetase by mutagenesis

M.R. Witmer, D. Palmieri-Young, and J.J. Villafranca

Three-dimensional model and quaternary structure of the human eye lens protein γS-crystallin based on β- and γ-crystallin X-ray coordinates and ultracentrifugation

S. Zarina, C. Slingsby, R. Jaenicke, Z.H. Zaidi, H. Driessen, and N. Srinivasan